

# Instability in crab crossing caused by interaction between beam loading on crab cavities and beam-beam force on colliding beams

Kazunori Akai 

High Energy Accelerator Research Organization (KEK), Tsukuba, Ibaraki 305-0801, Japan

 (Received 6 September 2023; accepted 27 October 2023; published 13 November 2023)

This study investigated an unknown instability in the crab-crossing scheme, which is caused by the interaction between beam loading on crab cavities and the coherent beam-beam force at the interaction point (IP). We developed an analysis method by formulating the transfer functions of the beam loading on the crab cavities and the related rf control loops, considering the beam-beam force on the colliding beams. The analysis was first applied to simple cases with no control loops to demonstrate the intrinsic stability of crab cavities under the beam loading and the beam-beam force, which corresponds to the Robinson stability for accelerating cavities. Furthermore, analysis with the control loops was applied to analyze unexpected oscillation phenomena observed in the crab-crossing operation in KEKB. The results obtained from the analysis were consistent with the observed phenomena at the following points: First, a time-domain simulation based on this analysis reproduced the observed coherent oscillation. Second, the relative orbit displacement between the colliding beams estimated in the analysis of the measured oscillation amplitude was consistent with the saturation effect of the beam-beam force at the IP. Third, rf-related parameter dependencies of stability obtained in the analysis were consistent with those in the measurements. The mechanism investigated in this study explained its essential function in the instability observed during the KEKB crab-crossing operation.

DOI: [10.1103/PhysRevAccelBeams.26.112001](https://doi.org/10.1103/PhysRevAccelBeams.26.112001)

## I. INTRODUCTION

A crab-crossing scheme was proposed in 1988 for linear colliders to recover head-on collisions in a finite-angle crossing scheme at the interaction point (IP) [1]. It has been shown that this scheme is also applicable to storage-ring colliders with a large crossing angle at the IP without the excitation of synchrotron-betatron resonances [2]. In later simulation works, the possibility of achieving a high beam-beam parameter  $\xi_y > 0.1$  was demonstrated by adopting this scheme [3,4]. Based on these studies, the crab-crossing scheme was first applied in KEKB to increase luminosity. KEKB is an asymmetric-energy double-ring collider comprising an 8-GeV electron ring (high-energy ring, HER) and a 3.5-GeV positron ring (low-energy ring, LER) [5]. The crab-crossing operation in KEKB for physics experiments started in 2007 and continued until 2010, when the operation was terminated to upgrade KEKB to SuperKEKB. The luminosity record of KEKB was obtained by crab crossing [6,7]. Crab-crossing and related systems

have been considered and are under development in a wide number of accelerators, including upgradation of LHC to HL-LHC, the Electron-Ion Collider, the linear colliders, and the generation of short-pulse x-rays in storage-ring-based light sources.

In the crab-crossing scheme, the bunches are tilted using radio-frequency (rf) deflecting cavities (crab cavities) to facilitate head-on collision at the IP despite a finite-angle crossing of the beam orbits, as shown in Fig. 1. Two superconducting crab cavities were fabricated for KEKB and

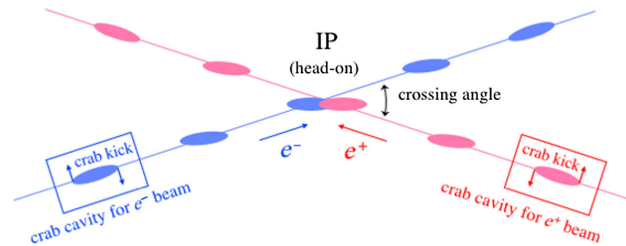


FIG. 1. Schematic of the crab-crossing scheme. The single crab cavity scheme is shown, where one crab cavity section is located in each ring. The  $e^+e^-$  bunches are tilted by transverse kick at the crab cavities. The betatron phase advance from the crab cavity to the IP is adjusted to  $\pi/2 + n\pi$ , where  $n$  is an integer. The crab voltage is adjusted to compensate for the crossing angle of beam orbits at the IP such that the beams collide head-on.

Published by the American Physical Society under the terms of the [Creative Commons Attribution 4.0 International license](https://creativecommons.org/licenses/by/4.0/). Further distribution of this work must maintain attribution to the author(s) and the published article's title, journal citation, and DOI.

installed in the LER and the HER, with one in each ring [8]. They successfully operated during the crab-crossing operation, contributing to an increase in luminosity.

However, an unexpected problem was encountered in the KEKB crab-crossing operation with high-current colliding beams. Large-amplitude coherent oscillation of the beams and crabbing field was observed, which caused unstable collision of beams and a reduction in luminosity. The cause was not fully understood; however, it was suspected to be related to beam loading on the crab cavities and the beam-beam force at the IP [9]. This problem was mitigated not to cause luminosity reduction by adjusting rf-related parameters to appropriate values that were experimentally determined during operation [9,10].

In this study, we investigated the instability driven by the interaction between the beam loading on the crab rf system and the beam-beam force at the IP. Although this study was motivated by the phenomena observed in the KEKB operation, the aim was to render the analysis applicable to other cases to the best extent possible. In Sec. II, we develop an analytical method by formulating the transfer functions (TF) of the crab rf system with beams, comprising the beam loading on crab cavities, beam-beam force at the IP, and rf control loops. In Sec. III, the analysis is applied to simple cases without control loops to derive an “intrinsic” stability criterion for a crab cavity with colliding beams, which corresponds to the Robinson stability for the accelerating cavities [11]. In Sec. IV, the analysis is applied to the KEKB operation with control loops. The calculation results were compared with the measurements to examine their consistency. Related discussions are presented in Sec. V and we conclude the study in Sec. VI.

## II. FORMULATION OF ANALYSIS METHOD

Crab crossing as shown in Fig. 1 is a single crab cavity scheme wherein one crab cavity section is located in each ring, and the bunches are tilted all around the ring. In a different crab-crossing scheme, two crab-cavity sections are located on both sides of the IP, and the bunch tilt is localized between the cavities (local crab scheme). The crossing plane can be either horizontal or vertical. Although the following analysis was conducted for the single crab cavity scheme with a horizontal crossing, it is applicable to the local crab scheme or the vertical crossing case with minor modifications.

To study the stability of the system, we first considered the steady state of the crab rf system with colliding beams under a set of operating conditions. We assumed that the following conditions are satisfied in steady state: (i) The beam in each ring ( $\pm$ ) passes the crab cavity at the crabbing phase  $\phi_c^\pm$ , which is the relative phase between the crabbing voltage  $V_c^\pm$  and beam, (ii) The beam does not necessarily pass on axis of the crab cavity. It may pass at an orbit displaced horizontally by  $\Delta x_{cr}^\pm$  from the cavity field

center, (iii) The amplitude and phase of  $V_c^\pm$  are maintained by control loops in the low-level rf (LLRF) system, and (iv) The relative horizontal orbit displacement of the two beams at the IP ( $\Delta x^{*+} - \Delta x^{*-}$ ) is adjusted to keep the collision by using, for example, a collision feedback system.

It is noted that the time constant of the collision feedback was assumed much slower than the oscillation period of the instability. In KEKB, the collision feedback was performed based on the beam-beam kick measured by beam position monitors around the IP, and the typical time constant of the feedback was 1 s [12], which was much slower than the observed oscillation period ( $\sim 2$  ms). So the only role of the collision feedback here is to set the operating beam orbit appropriately in steady state, and its dynamical effect is not considered in our analysis. Hereafter, the superscript or subscript of  $\pm$  representing the ring may be omitted if it is clear or unnecessary in context.

Next, the effect of small signal fluctuations from the steady state was analyzed using TFs. Figure 2 shows a block diagram of a crab rf system with colliding beams. In the case of crab cavities, in contrast to the case in accelerating cavities, the beam loading on the cavity is proportional to  $\Delta x_{cr}$ , as described in Sec. II A. The TFs corresponding to the beam loading from  $\Delta x_{cr}$  onto the amplitude and phase of  $V_c$  are represented by  $G_{xa}^B$  and  $G_{xp}^B$ , respectively.  $\Delta k_{cr}^\pm$  is the deviation of the kick at the bunch center in the crab cavity. The TFs from  $\Delta k_{cr}$  of ring

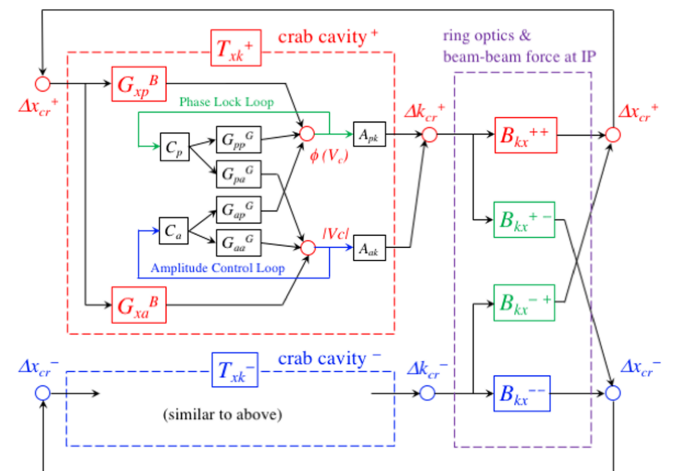


FIG. 2. Block diagram of crab rf system with colliding beams.  $B_{kx}^{MN}$  is the TF from the kick on the bunch center at crab cavity  $\Delta k_{cr}$  of the ring  $M$  to the orbit displacement at crab cavity  $\Delta x_{cr}$  of the ring  $N$ .  $G_{xa}^B$  and  $G_{xp}^B$  are the TFs corresponding to the beam loading, from  $\Delta x_{cr}$  to the amplitude and phase of  $V_c$ , respectively. The TFs from rf generator to the cavity ( $G_{ap}^G$ ) and the amplitude and phase control functions ( $C_a$  and  $C_p$ ) are also included. By focusing on  $\Delta x_{cr}^\pm$  and  $\Delta k_{cr}^\pm$ , the system can be grouped into three parts,  $T_{xk}^+$ ,  $T_{xk}^-$ , and a set of  $B_{kx}^{MN}$ , as surrounded by dotted lines.

$M$  to  $\Delta x_{cr}$  of ring  $N$  are represented as  $B_{kx}^{MN}$ , where  $M$  and  $N$  are  $+$  or  $-$ . The form of  $B_{kx}^{MN}$  was determined from the coherent beam-beam force at the IP and the optical parameters of the rings, as described in Sec. II B. In addition to beam loading, each crab rf system includes the TFs from rf generator to the cavity ( $G_{\alpha\beta}^G$ , where  $\alpha$  and  $\beta$  are either  $a$  or  $p$ ) and the TFs of amplitude and phase control functions ( $C_a$  and  $C_p$ ). These are described in Sec. II C.

Note that the phase and amplitude deviations of  $V_c$  affect both  $\Delta k_{cr}$  and the bunch tilt. However, a small change in the bunch tilt does not significantly affect the beam loading or coherent beam-beam kick at the IP. Consequently, the tilt change was not considered in our analysis, and the corresponding TFs from  $V_c$  to the tilt are not represented in the block diagram.

By focusing on  $\Delta x_{cr}^\pm$  and  $\Delta k_{cr}^\pm$ , the system can be grouped into three parts,  $T_{xk}^+$ ,  $T_{xk}^-$ , and a set of  $B_{kx}$ 's, as surrounded by dotted lines in the figure. The characteristic equation (CE) for these TFs is

$$\begin{aligned}
 0 = & 1 - T_{xk}^+ B_{kx}^{++} - T_{xk}^- B_{kx}^{--} \\
 & + T_{xk}^+ T_{xk}^- (B_{kx}^{++} B_{kx}^{--} - B_{kx}^{+-} B_{kx}^{-+}). \quad (1)
 \end{aligned}$$

### A. Beam loading on the crab cavity

First, we formulated the TFs for the beam loading on the crab cavities  $G_{xa}^B$  and  $G_{xp}^B$ . This was performed in a manner similar to that for accelerating cavities studied by Pedersen [13]. The following differences were considered: (i) The beam-induced voltage in the crab cavity is dependent on the horizontal beam orbit in the cavity  $\Delta x_{cr}$  and that in the accelerating cavity is not. (ii) The beam-induced voltage in the crab cavity (accelerating cavity) is in the transverse (longitudinal) direction, thus its phase on resonance is  $\pm 90^\circ$  ( $180^\circ$ ) with respect to the beam. (iii) The longitudinal position of beam is determined by the accelerating cavities, thus the synchronous phase  $\phi_s$  is not involved in this analysis. Instead, the crabbing phase  $\phi_c$  plays an important role.

Figure 3 shows the vector relation representing the beam loading on the crab cavity. The  $x$ -axis represents the reference phase defined by the timing of the bunch center passing the crab cavity, that is, the beam phase. The projection of  $V_c$  vector on the  $x$ -axis ( $y$ -axis) gives the kick voltage (tilt force) to the bunch center. Here, we consider the case wherein the phase advance from the crab cavity to the IP is close to  $\pi/2 + 2n\pi$ , where  $n$  is an integer. (The case of  $3\pi/2 + 2n\pi$  can be treated similarly.) As the bunch head (tail) passes the cavity earlier (later) than the bunch center does, the bunch head (tail) is kicked in the inward (outward) direction of the ring compared to the bunch center. The signs of  $\Delta x_{cr}^\pm$  and  $\Delta k_{cr}^\pm$  are defined as positive when they are directed inside the ring. The beam

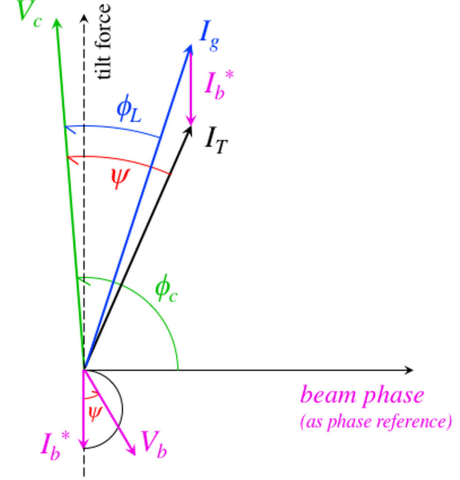


FIG. 3. Vector relation for the beam loading current  $\mathbf{I}_b^*$ , the generator current  $\mathbf{I}_g$ , and the crabbing voltage  $\mathbf{V}_c$ , representing the beam loading on crab cavities.  $\mathbf{I}_b^*$  is dependent on  $\Delta x_{cr}$  and its phase is  $\pm 90^\circ$  with respect to the beam phase.  $\phi_c$  is the crabbing phase, the phase of  $\mathbf{V}_c$  with respect to the beam phase.  $\phi_L$  is the loading angle, the relative phase between  $\mathbf{I}_g$  and  $\mathbf{V}_c$ .  $\psi$  is the tuning angle, the relative phase between  $\mathbf{I}_T$  and  $\mathbf{V}_c$ , where  $\mathbf{I}_T = \mathbf{I}_g + \mathbf{I}_b^*$ . The impedance (the ratio of voltage to current) is set 1.5 on this diagram.

loading current  $\mathbf{I}_b^*$  is related to the dc beam current  $I_b$ : for small values of  $|\Delta x_{cr}|$ ,  $|\mathbf{I}_b^*| = I_b k_{rf} |\Delta x_{cr}|$ , where  $k_{rf}$  is the rf wave number. The vector  $\mathbf{I}_b^*$  lies along the vertical axis in the figure and is directed downward (upward) when  $\Delta x_{cr} > 0$  ( $\Delta x_{cr} < 0$ ). The same vector relationship can be used regardless of the sign of the charged particles.

From the vector relation, the relationship between the amplitude and phase deviations of the generator current  $\mathbf{I}_g$ :  ${}^t(a_g, p_g)$ , beam loading current  $\mathbf{I}_b^*$ :  ${}^t(a_b, p_b)$ , and crabbing voltage  $\mathbf{V}_c$ :  ${}^t(a_v, p_v)$  is expressed as

$$\begin{pmatrix} a_v \\ p_v \end{pmatrix} = \mathbf{G} \left[ \frac{I_g}{I_T} \mathbf{R}(\theta_g) \begin{pmatrix} a_g \\ p_g \end{pmatrix} + \frac{I_b^*}{I_T} \mathbf{R}(\theta_b) \begin{pmatrix} a_b \\ p_b \end{pmatrix} \right], \quad (2)$$

where  $\mathbf{G}$  corresponds to the cavity impedance, which is expressed as

$$\mathbf{G} = \begin{pmatrix} G_s & G_c \\ -G_c & G_s \end{pmatrix}, \quad (3)$$

with

$$G_s(s) = \frac{\sigma s + \sigma^2 \sec^2 \psi}{s^2 + 2\sigma s + \sigma^2 \sec^2 \psi}, \quad (4)$$

$$G_c(s) = \frac{\sigma s \tan \psi}{s^2 + 2\sigma s + \sigma^2 \sec^2 \psi}, \quad (5)$$

where  $\sigma$  and  $\psi$  are the damping rate and the tuning angle, respectively, of crab cavity.  $\mathbf{I}_T$  is the total current:  $\mathbf{I}_T = \mathbf{I}_g + \mathbf{I}_b^*$ .  $I_g = |\mathbf{I}_g|$ ,  $I_T = |\mathbf{I}_T|$ , and  $I_b^* = I_b k_{rf} \Delta x_{cr} = |\mathbf{I}_b^*|$  for  $\Delta x_{cr} > 0$  ( $= -|\mathbf{I}_b^*|$  for  $\Delta x_{cr} < 0$ ).  $\mathbf{R}$  denotes the rotation matrix as

$$\mathbf{R}(\theta) = \begin{pmatrix} \cos \theta & \sin \theta \\ -\sin \theta & \cos \theta \end{pmatrix}, \quad (6)$$

and  $\theta_b = \pi/2 + \phi_c - \psi$  and  $\theta_g = \phi_L - \psi$ , where  $\phi_L$  is the loading angle, which is the relative phase between  $\mathbf{I}_g$  and  $\mathbf{V}_c$ . Also from the vector relation, the relationships between  $I_T$ ,  $I_g$ , and  $I_b^*$  are expressed as

$$\frac{I_g}{I_T} = \frac{\cos \psi}{\cos \phi_L} (1 + Y^* \sin \phi_c), \quad (7)$$

$$\frac{I_b^*}{I_T} = Y^* \cos \psi, \quad (8)$$

where  $Y^*$  is represented as

$$Y^* = \left(\frac{R}{Q}\right) Q_L I_b^* / V_c = \left(\frac{R}{Q}\right) Q_L I_b k_{rf} \Delta x_{cr} / V_c, \quad (9)$$

where  $R/Q$  and  $Q_L$  are the  $R/Q$  and loaded  $Q$  values of crab cavity, respectively. Here, the definition of  $R/Q = V_c^2 / \omega_{rf} U$  was used, where  $\omega_{rf}$  is the angular rf frequency and  $U$  is the stored energy. The transformation from vector  ${}^t(a_b, p_b)$  to  ${}^t(a_v, p_v)$  yielded the TFs from  $\mathbf{I}_b^*$  to  $\mathbf{V}_c$ . Because  $a_b$  is proportional to  $\Delta x_{cr}$ , we focused on the TFs from  $\Delta x_{cr}$  to  $\mathbf{V}_c$ , which were obtained using the coefficients in Eq. (9),  $Y' \equiv Y^* / \Delta x_{cr}$ , as:

$$G_{xa}^B = \frac{-\sigma Y' \sin \phi_c \cdot s + \sigma^2 Y' (\tan \psi \cos \phi_c - \sin \phi_c)}{s^2 + 2\sigma s + \sigma^2 \sec^2 \psi}, \quad (10)$$

$$G_{xp}^B = \frac{-\sigma Y' \cos \phi_c \cdot s - \sigma^2 Y' (\tan \psi \sin \phi_c + \cos \phi_c)}{s^2 + 2\sigma s + \sigma^2 \sec^2 \psi}. \quad (11)$$

Note that the beam phase is determined by the accelerating rf system, and the accelerating and crab rf systems are independently controlled. In addition, the crab kick is in the transverse direction and does not affect the longitudinal motion. Consequently, the deviation of the phase of  $\mathbf{I}_b^*$  ( $p_b$ ) is not important in this analysis, and the corresponding TFs from  $p_b$  to  $V_c$ ,  $G_{pp}^B$  and  $G_{pa}^B$ , were not used in the subsequent analysis. (One exceptional case is discussed in Sec. V.)

### B. Effective orbit response to crab kick with beam-beam force at the IP

Next, we formulated  $B_{kx}$  values, which are the TFs from the kick  $\Delta k_{cr}$  to orbit displacement  $\Delta x_{cr}$ , considering the

beam-beam force at the IP. Let the kick step change at the 0th turn from steady state to  $\Delta k_{cr}^\pm$ , and we tracked the horizontal orbit changes in the crab cavities  $\Delta x_{cr}^\pm$ . The transformation of the vector  ${}^t(\Delta x_{cr}^+, \Delta x_{cr}'^+, \Delta x_{cr}^-, \Delta x_{cr}'^-)$  from the  $N$ th turn to the  $(N+1)$ th turn is expressed as

$$\begin{pmatrix} \Delta x_{cr}^+ \\ \Delta x_{cr}'^+ \\ \Delta x_{cr}^- \\ \Delta x_{cr}'^- \end{pmatrix}^{(N+1)} = T \times \begin{pmatrix} \Delta x_{cr}^+ \\ \Delta x_{cr}'^+ \\ \Delta x_{cr}^- \\ \Delta x_{cr}'^- \end{pmatrix}^{(N)} + \begin{pmatrix} 0 \\ \Delta k_{cr}^+ \\ 0 \\ \Delta k_{cr}^- \end{pmatrix}. \quad (12)$$

The  $4 \times 4$  matrix  $T$  for the transformation is expressed as

$$T = \begin{pmatrix} \mathbf{M}_{21}^+ & \mathbf{0} \\ \mathbf{0} & \mathbf{M}_{21}^- \end{pmatrix} \times R \times \begin{pmatrix} \mathbf{M}_{12}^+ & \mathbf{0} \\ \mathbf{0} & \mathbf{M}_{12}^- \end{pmatrix}, \quad (13)$$

where  $\mathbf{M}_{12}^\pm$  and  $\mathbf{M}_{21}^\pm$  are  $2 \times 2$  transfer matrices from the crab cavity to the IP and from the IP to the crab cavity, respectively, and  $R$  is a  $4 \times 4$  matrix that describes the beam-beam transformation at the IP.

To express  $R$ , we used the formula obtained from the analysis of coherent dipole oscillation mode in a rigid Gaussian model presented in Ref. [14]. The coherent beam-beam kick was parametrized by the coherent beam-beam parameter  $\Xi_x^\pm$  defined as

$$\Xi_x^\pm = \frac{N^\mp r_e}{\gamma^\pm} \frac{\beta_x^{*\pm}}{2\pi \Sigma_x (\Sigma_x + \Sigma_y)}, \quad (14)$$

where  $r_e$  is the classical radius of the particles,  $N$  is the number of particles in a bunch,  $\gamma$  is the Lorentz energy factor, and  $\beta_x^*$  is the horizontal beta function at the IP.  $\Sigma_x = \sqrt{(\sigma_x^+)^2 + (\sigma_x^-)^2}$  and  $\Sigma_y = \sqrt{(\sigma_y^+)^2 + (\sigma_y^-)^2}$  are the horizontal and vertical effective beam sizes at the IP, respectively, where  $\sigma_x^\pm$  and  $\sigma_y^\pm$  are the beam sizes of each beam at the IP. In our coordinate system,  $R$  is expressed as

$$R = I + 4\pi \begin{pmatrix} 0 & 0 & 0 & 0 \\ -\frac{\Xi_x^+}{\beta_x^{*+}} & 0 & \frac{\Xi_x^+}{\beta_x^{*+}} \sqrt{\frac{\beta_x^{*-}}{\beta_x^{*+}}} & 0 \\ 0 & 0 & 0 & 0 \\ \frac{\Xi_x^-}{\beta_x^{*-}} \sqrt{\frac{\beta_x^{*+}}{\beta_x^{*-}}} & 0 & -\frac{\Xi_x^-}{\beta_x^{*-}} & 0 \end{pmatrix}, \quad (15)$$

where  $I$  denotes a unit matrix. The new steady state with  $\Delta k_{cr}^\pm$  is obtained by setting  $N \rightarrow \infty$  as follows:

$$\begin{pmatrix} \Delta x_{cr}^+ \\ \Delta x_{cr}'^+ \\ \Delta x_{cr}^- \\ \Delta x_{cr}'^- \end{pmatrix}^{(\infty)} = (I - T)^{-1} \times \begin{pmatrix} 0 \\ \Delta k_{cr}^+ \\ 0 \\ \Delta k_{cr}^- \end{pmatrix}. \quad (16)$$

To determine  $B_{kx}$ , we assumed that the following two conditions are satisfied: (1) Machine operation is performed below the well-known beam-beam limit for the coherent  $\sigma$ - and  $\pi$ -mode instability of colliding beams, which is determined from the trace of the matrix  $T$ . In this case, the disturbed beam orbit converges to a new steady state after the radiation damping time  $\tau_{\text{rad}}$ . (2) The filling time of the crab cavity  $\tau_f$  is much longer than the time of one-turn revolution period  $\tau_{\text{rev}}$ . In this case, beam loading is evaluated by integrating the beam-induced voltage for multiple turns with the decay time constant  $\tau_f$ . Because the beam-induced voltage is proportional to  $\Delta x_{cr}$ , as described in the previous section, it is equivalent to evaluating the ‘‘effective’’ orbit response, which is the integrated orbit response for multiple turns with a decay time constant  $\tau_f$ .

These assumptions were satisfied in the KEKB case: the first point was evident from the operational parameters. The second condition was satisfied because  $\tau_f$  of the LER (HER) crab cavity was  $12.5 \tau_{\text{rev}}$  ( $10.0 \tau_{\text{rev}}$ ), where  $\tau_{\text{rev}} \sim 10 \mu\text{s}$ . The justification for using an effective orbit response instead of a turn-by-turn response should be noted here. In another work at KEKB, coherent excitation of the  $\sigma$ - and  $\pi$ -mode oscillations via the application of sinusoidal rf phase modulation was studied experimentally and by simulation [15]. The modulation frequencies were chosen 40–50 kHz to resonantly excite these modes. The turn-by-turn change in the horizontal orbit at these high frequencies was considered; however, the beam loading on the crab cavities was outside the scope of their study. In our study, however, coherent excitation with a heavy beam-loading effect was a concern. The typical time constant of the observed oscillation was on the order of  $200 \tau_{\text{rev}}$ , which is much longer than  $\tau_f$ . This is a rather static phenomenon from the perspective of turn-by-turn change. Therefore, these two separate studies address different issues, and it is justified to use an effective orbital response in our analysis.

The orbital response to a step-kick change was simulated for the KEKB case. Because the horizontal tune  $\nu_x$  was chosen to be closed to a half integer, the orbit oscillated turn-by-turn with a period of approximately two turns after the kick change until it converged in  $\tau_{\text{rad}}$  ( $\sim 4000$  turns). However, the effective orbit converged significantly faster, as shown in Fig. 4. The effective orbit responses in the LER cavity to a step-kick change applied to the LER (HER) cavity at the 0th turn are plotted as red (blue) real lines. The corresponding new steady orbits after  $\tau_{\text{rad}}$  were calculated using Eq. (16) and are indicated by dotted straight lines. The effective orbits almost converged to the new steady orbits in around  $\tau_f$ . Although the turn-by-turn change with a period of two turns was still observed in the effective orbits, it was considerably smaller than the change to the new steady orbit. The convergence would be even faster owing to the bunch-by-bunch transverse feedback system.

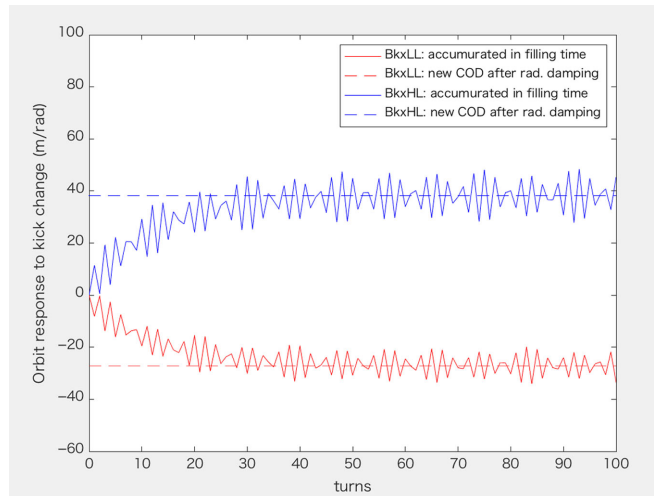


FIG. 4. Response of the beam orbit in the LER crab cavity to a step change of kick applied in the LER (HER) cavity at the 0th turn, plotted in red (blue). The effective orbits, obtained by integrating the orbit for multiple turns with a decay time constant  $\tau_f$  (12.5 turns), are plotted in real lines. The new steady orbits calculated using Eq. (16) are plotted by dotted lines. The horizontal axis is the turns.

In the KEKB operation, the damping time of the feedback system was nominally set around  $500 \mu\text{s}$  (50 turns) [16].

Consequently,  $B_{kx}$  values were formulated with an effective orbit response and can be modeled with the matrix  $(I - T)^{-1}$  and the first-order delay function with a time constant  $\tau_f$  as

$$B_{kx}^{mn} = B_{kx,0}^{mn} \times \frac{1}{1 + \tau_f s}, \quad (17)$$

$$B_{kx,0}^{mn} = [(I - T)^{-1}]_{(n,m+1)}, \quad (18)$$

where  $[X]_{(a,b)}$  denotes the  $(a, b)$  component of matrix  $X$  and the + beam is represented by  $m = n = 1$  and the - beam by  $m = n = 3$ . When the timescale of the phenomenon is significantly slower than  $\tau_f$ ,  $B_{kx,0}^{mn}$  can be used instead of  $B_{kx}^{mn}$ .

### C. rf system with control loops

As shown in Fig. 2,  $T_{xk}$  includes the rf control part, in addition to the beam loading  $G_{xa}^B$  and  $G_{xp}^B$ . The rf control part includes the control functions of the amplitude control loop (ACL)  $C_a$  and phase-lock loop (PLL)  $C_p$  and the TFs from the generator to the cavity  $G_{\alpha\beta}^G$ , where  $\alpha$  and  $\beta$  are  $a$  or  $p$ . The forms of  $C_a$  and  $C_p$  are determined according to the control loop circuits specific to the system.  $G_{\alpha\beta}^G$  was obtained by transforming  ${}^t(a_g, p_g)$  into  ${}^t(a_v, p_v)$  in Eq. (2); the results are presented in Appendix A. They are similar to those of accelerating cavities [13,17], with differences in the beam loading coefficients and phase between the rf and

beam. The TF from the phase and amplitude of  $V_c$  to the kick  $A_{pk}$  and  $A_{ak}$ , respectively, are expressed as

$$A_{pk} = -\frac{eV_c}{E} \sin \phi_c, \quad \text{and} \quad A_{ak} = \frac{eV_c}{E} \cos \phi_c. \quad (19)$$

where  $G_{\alpha\beta}^B$ ,  $G_{\alpha\beta}^G$ , and  $A_{\alpha k}$ , with  $\alpha$  and  $\beta$  being  $a$  or  $p$ , are shown in Eqs. (10) and (11), Eqs. (A1) and (A2), and Eq. (19), respectively.

For later discussion,  $T_{xk}$  for three simple cases with no loops, only the PLL, and only the ACL are derived. Without loops ( $C_a = C_p = 0$ ), Eq. (20), using Eqs. (10) and (11), is reduced to a simple form as follows:

$$T_{xk} = T_{xk,0} \times \tan \psi, \quad (21)$$

where

$$T_{xk,0} \equiv \frac{\sigma^2 Y'}{s^2 + 2\sigma s + \sigma^2 \sec^2 \psi} \times \frac{eV_c}{E}. \quad (22)$$

In this case,  $T_{xk}$  depends on  $\psi$  and not on  $\phi_c$  or  $\Delta x_{cr}$ . In contrast, in cases with only the PLL ( $C_a = 0$ ) or only the ACL ( $C_p = 0$ ), Eq. (20) reduces to

$$T_{xk} = T_{xk,0} \times \frac{\sin \psi - C_p [\sin(\phi_c - \psi) + Y^* \cos \psi] \cos \phi_c}{\cos \psi (1 + C_p G_{pp}^G)} \quad (23)$$

or

$$T_{xk} = T_{xk,0} \times \frac{\sin \psi + C_a \cos(\phi_c - \psi) \sin \phi_c}{\cos \psi (1 + C_a G_{aa}^G)}, \quad (24)$$

respectively. Thus, with feedback loops,  $T_{xk}$  is dependent on  $\psi$ ,  $\phi_c$ ,  $\Delta x_{cr}$ , and the parameters related to  $C_a$  and  $C_p$ .

It is noted that the tuning control is usually performed based on the loading angle  $\phi_L$ . The measured phase in the tuning control system is  $\phi_L$  and not  $\psi$ . The relationship between  $\phi_L$  and  $\psi$  is obtained from the vector relationship as

$$\tan \psi = (1 + Y^* \sin \phi_c) \tan \phi_L + Y^* \cos \phi_c. \quad (25)$$

In the case of crab cavities, the difference between  $\psi$  and  $\phi_L$  is typically small, because  $Y^*$  ( $= Y' \Delta x_{cr}$ ) is much smaller than one. Therefore, we used  $\psi$  in the following analysis unless  $\phi_L$  was required in this context. In addition, the TF for the tuning control loop was not explicitly

where  $e$  denotes the electric charge and  $E$  denotes the beam energy.

By combining these components according to Fig. 2 and performing appropriate transformations, or equivalently by applying Mason's rule,  $T_{xk}$  can be represented as

$$T_{xk} = \frac{G_{xp}^B [(1 + C_a G_{aa}^G) A_{pk} - C_p G_{pa}^G A_{ak}] + G_{xa}^B [(1 + C_p G_{pp}^G) A_{ak} - C_a G_{ap}^G A_{pk}]}{1 + C_a G_{aa}^G + C_p G_{pp}^G + C_a C_p (G_{aa}^G G_{pp}^G - G_{ap}^G G_{pa}^G)}, \quad (20)$$

included in our analysis because its time constant is usually slow compared to the typical time constant of beam oscillation. Regarding the rf power required to maintain  $V_c$  at  $\phi_L$  with a non-negligible value of  $Y^*$ , a formalism has been reported elsewhere [18].

### III. INTRINSIC STABILITY

The analysis described in the previous section was first applied to simple cases without control loops. In other words, we discuss the intrinsic stability of the crab system, which is determined by the interaction between the beam loading on the crab cavities and the beam-beam force at the IP. This corresponds to the Robinson stability for the accelerating cavities, wherein stability under the beam loading on accelerating cavities without control loops was studied [11].

First, we examined a special case wherein every machine parameter, except the charge sign, is identical for the two rings. This facilitated easy extraction of the essence of intrinsic stability with less complicated mathematics. In this case,  $T_{xk}^+ = T_{xk}^- (= T_{xk})$ ,  $B_{kx}^{++} = B_{kx}^{--} (= B_{kx})$ , and  $B_{kx}^{+-} = B_{kx}^{-+}$ . Subsequently, the CE represented in Eq. (1) becomes

$$0 = [1 - T_{xk} B_{kx} (1 - \eta)] \times [1 - T_{xk} B_{kx} (1 + \eta)], \quad (26)$$

where  $\eta$  is defined as follows:

$$\eta \equiv \sqrt{\frac{B_{kx}^{+-} B_{kx}^{-+}}{B_{kx}^{++} B_{kx}^{--}}}. \quad (27)$$

Thus, CE is reduced to two simple equations:

$$0 = 1 - T_{xk} B_{kx} (1 \pm \eta). \quad (28)$$

We considered the case of slow dynamics compared with  $\tau_f$ , that is,  $B_{kx,0}$  [Eq. (18)] was used instead of  $B_{kx}$  [Eq. (17)]. In this case, with  $T_{xk}$  obtained for the no-control loops [Eqs. (21) and (22)], CE are converted to two quadratic equations:

$$s^2 + 2\sigma s + \sigma^2 [\sec^2 \psi - Y' \kappa B_{kx,0} \tan \psi (1 \pm \eta)] = 0, \quad (29)$$

where  $\kappa = eV_c/E$ . The four solutions to these two equations are obtained as follows:

$$s = -\sigma \pm \sigma \sqrt{-\tan^2 \psi + Y' \kappa B_{kx,0} \tan \psi (1 \pm \eta)}. \quad (30)$$

The system is stable when the real parts of the four solutions are all negative. The stability criterion results in different forms depending on  $\eta < 1$  or  $\eta > 1$  as follows:

$$Y' \kappa B_{kx,0} \sin 2\psi < \frac{2}{1 + \eta} \quad \text{for } 0 < \eta < 1, \quad (31)$$

$$-\frac{2}{\eta - 1} < Y' \kappa B_{kx,0} \sin 2\psi < \frac{2}{1 + \eta} \quad \text{for } \eta > 1. \quad (32)$$

To indicate the stability criteria more specifically,  $B_{kx,0}$  and  $\eta$  were evaluated using Eqs. (13), (15), and (18) for the identical two rings. A more detailed derivation is provided in Appendix B and the results are represented as

$$B_{kx,0} = \frac{\beta_{cr} \{ \sin \phi_0 - 4\pi \Xi_x [\cos \varepsilon_{12} \cos \varepsilon_{21} - \cos^2(\phi_0/2)] \}}{2(1 - \cos \phi_0 + 4\pi \Xi_x \sin \phi_0)} \quad (33)$$

and

$$\eta = \left| \frac{4\pi \Xi_x [\cos \varepsilon_{12} \cos \varepsilon_{21} + \cos^2(\phi_0/2)]}{\{ \sin \phi_0 - 4\pi \Xi_x [\cos \varepsilon_{12} \cos \varepsilon_{21} - \cos^2(\phi_0/2)] \}} \right|, \quad (34)$$

where  $\beta_{cr}$  is the beta function at the crab cavity, and the betatron phase advances are defined as  $(\pi/2 + \varepsilon_{12})$  from the crab cavity to the IP,  $(\pi/2 + \varepsilon_{21})$  from the IP to the crab cavity, and  $\phi_0 = 2\pi\nu_x = \pi + \varepsilon_{12} + \varepsilon_{21}$  for one-turn of the ring, respectively. In a typical crab-crossing operation,  $|\varepsilon_{12}| \ll 1$ ,  $|\varepsilon_{21}| \ll 1$ , and  $\phi_0$  is close to  $\pi$ . In this case, as  $\Xi_x$  increases,  $B_{kx,0}$  and  $\eta$  approach  $-\pi \Xi_x \beta_{cr}$  and 1, respectively.

The stability criteria obtained using Eqs. (31) and (32) are shown in Fig. 5. The horizontal and vertical axes represent  $Y' \kappa B_{kx,0}$  and  $\psi$ , respectively. The two cases for  $\eta = 0.8$  and  $\eta = 1.2$  are indicated in red and blue, respectively. The stable and unstable regions are marked for these two cases. Here,  $Y' \kappa B_{kx,0}$  is approximately proportional to  $I_b^2$  until  $\Xi_x$  reaches the beam-beam limit because  $Y' \propto I_b$  and  $B_{kx,0} \propto \Xi_x$ . Moreover, the stable region for  $\psi$  is dependent on the sign of  $B_{kx,0}$ . As shown in Eq. (33), the sign of  $B_{kx,0}$  can differ between small and large values of  $\Xi_x$ . The sign of  $B_{kx,0}$  is also dependent on the relative charge sign of the two beams. When the two beams have opposite (same) charge sign, the beam-beam force at the IP is attractive (repulsive). In the expressions

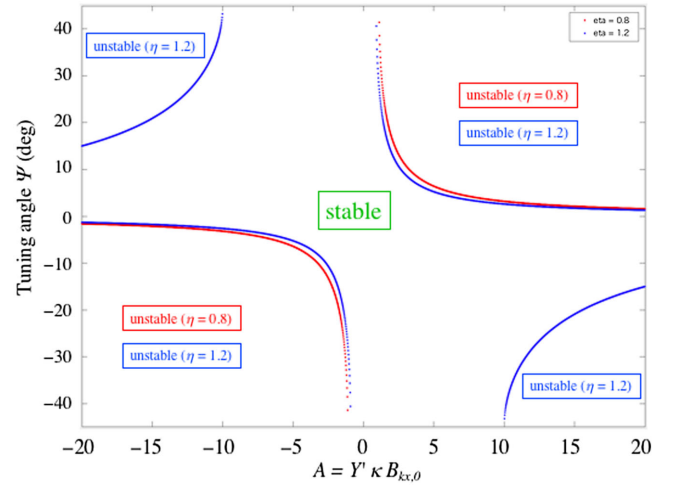


FIG. 5. Intrinsic stability of the crab system without control loops for the case wherein every machine parameter is identical for the two rings. The horizontal and vertical axes are  $Y' \kappa B_{kx,0}$  and  $\psi$ , respectively. Unstable regions for the two cases of  $\eta = 0.8$  (red) and  $\eta = 1.2$  (blue) are shown.

for  $R$  in Eq. (15), it was implied that the two beams had opposite charge signs. Therefore, the results obtained in this section can be used for the same charge sign case by replacing  $\Xi_x$  with  $-\Xi_x$ . For large values of  $\Xi_x$ ,  $B_{kx,0} < 0$  ( $B_{kx,0} > 0$ ) with the opposite (same) charge sign case.

Next, the KEKB case was examined as an example of a general case for two rings with different parameters.  $B_{kx,0}$  was used instead of  $B_{kx}$  also in this case. The fourth-order CE [Eq. (1)] was solved for different values of the tuning angle of LER  $\psi_L$  and that of HER  $\psi_H$ . The beam currents in LER ( $I_{b(L)}$ ) and HER ( $I_{b(H)}$ ) were changed with a fixed ratio  $I_{b(L)}/I_{b(H)} = 2$ . The other parameters were set to those used in the operation, which are presented in the next section. The maximum LER beam current ( $I_{b(L)\max}$ ), for which the real parts of the four solutions were all negative, was obtained at the given values of  $\psi_L$  and  $\psi_H$ . Figure 6 shows  $I_{b(L)\max}$  as a function of  $\psi_L$  (horizontal axis) and  $\psi_H$  (vertical axis). It is seen that  $I_{b(L)\max}$  decreased for lower values of  $\psi_L$  or  $\psi_H$ . This tendency was similar to that of the two identical ring case shown in Fig. 5 with  $Y' \kappa B_{kx,0} < 0$ .

As described previously, the two parameters  $Y' \kappa B_{kx,0}$  and  $\psi$  are essential for the intrinsic stability of the crab system. Regarding intrinsic stability, the system is always stable at  $\psi = 0$  for the two identical ring cases (Fig. 5) and the system is stable with  $I_{b(L)} = 2$  A and  $I_{b(H)} = 1$  A for any value of  $|\psi_L| < 30^\circ$  and  $|\psi_H| < 30^\circ$  in the KEKB case (Fig. 6). However, the stability with the control loops can be affected by other rf parameters and control loops. In addition, in real machines, stability can be degraded by a variety of nonideal conditions such as machine errors and nonlinearities. The following sections discuss these points.

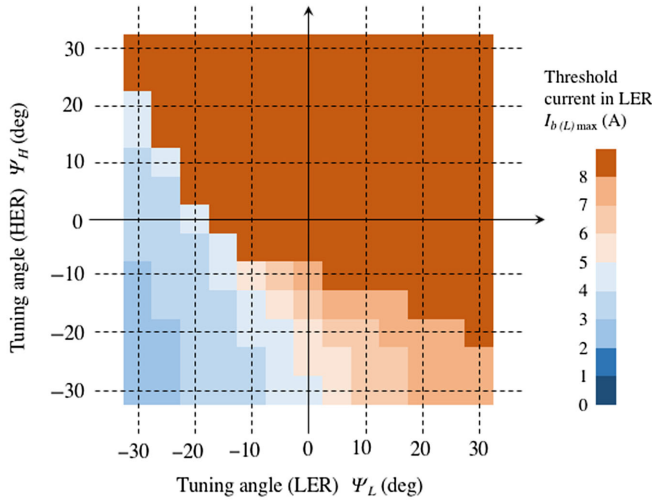


FIG. 6. Threshold beam current for the intrinsic stability in the KEKB case, as an example of two rings with different parameters. The maximum LER beam current is shown, with a fixed ratio  $I_{b(L)}/I_{b(H)} = 2$ . The horizontal and vertical axes are  $\psi_L$  and  $\psi_H$ , respectively.

#### IV. CRAB-CROSSING OPERATION IN KEKB

##### A. Observed oscillation phenomena

Table I lists the machine parameters for the crab-crossing operation in KEKB as of June 2007 [6,9]. The parameters in this period were chosen because intensive observations of the oscillation phenomena and related machine studies were conducted during this period. The numbers in parentheses indicate those at the final stage of operation in 2010 [7]. During the operation, the amplitude of the

TABLE I. Machine parameters with the crab-crossing operation in KEKB as of June 2007 [6,9]. The numbers in parenthesis show those at the final stage of operation in 2010 [7].

Parameter	Unit	LER	HER
Beam particles		$e^+$	$e^-$
Beam energy	(GeV)	3.5	8.0
Beam current	(mA)	1150 (1637)	620 (1188)
No. of bunches		1389 (1585)	
$\beta_x^*$ at IP	(m)	0.9 (1.2)	0.9 (1.2)
$\beta_x$ at crab	(m)	80 (51)	170 (122)
$\sigma_x^*$	( $\mu\text{m}$ )	116	147
$\sigma_y^*$	( $\mu\text{m}$ )	1.1 (0.94)	1.1 (0.94)
$\nu_x$		0.505	0.509
Crossing angle <sup>a</sup>	(mrad)		22
rf frequency	(MHz)		508.9
Revolution freq.	(kHz)		99.4
No. of crab cavities		1	1
$R/Q$ of cavity	( $\Omega$ )	47	47
Loaded- $Q$ ( $Q_L$ )	( $\times 10^5$ )	2.0	1.6
Crab voltage	(MV)	0.90 (0.97)	1.43 (1.45)

<sup>a</sup>Crossing angle of beam orbits.

crabbing voltage  $V_c$  was adjusted to provide the required kick for head-on collisions with a crossing angle of 22 mrad of the beam orbits. The nominal crabbing phase  $\phi_c = 90^\circ$ , where the bunch center passed the cavity at the zero cross of  $V_c$ , was determined by measuring the beam orbit change by crabbing on and off. The beam orbit in the cavity was adjusted on axis of the crabbing field to minimize the beam loading current  $I_b^*$  by measuring rf power as a function of the dc beam current  $I_b$ . These conditions were fine-tuned to optimize the luminosity and beam performances. The beam operation was always performed at beam currents sufficiently lower than the well-known limit for the coherent  $\sigma$ - and  $\pi$ -mode instability of colliding beams, as mentioned in Sec. II B. Further details of the system description and operation status have been reported elsewhere [6–9].

Figure 7 shows an example of the oscillations observed in the LER cavity. The amplitude and phase of  $V_c$  oscillated at approximately 550 Hz. Oscillation was also observed in the HER cavity; the oscillation phase was almost antiphase with respect to the LER cavity. The oscillating input power suggests that the rf control loops were involved in this phenomenon. Oscillation resulted in unstable horizontal orbits of the two beams at the IP and considerable luminosity degradation. This phenomenon occurred only when high-current beams were stored in both rings, and never occurred with a single beam or low-current beams.

During operation, it was suspected that this phenomenon might be related to the possible interaction between the beam loading on the crab cavities and the beam-beam force at the IP. Subsequently, the effect of changing rf-related parameters, such as  $\phi_c$ ,  $\psi$ , and  $V_c$ , as well as the feedback parameters, on stability was studied. Shifting the  $\phi_c$  and  $\psi$  from their nominal values ( $\phi_c = 90^\circ$  and  $\psi = 0^\circ$ ) significantly affected the stability. Specifically, setting  $\phi_c = 100^\circ$

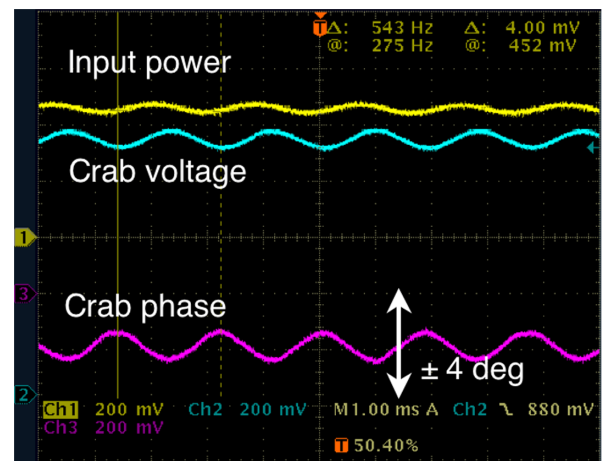


FIG. 7. An example of the observed oscillation in the KEKB crab-crossing operation. The input power,  $V_c$  amplitude, and the crabbing phase  $\phi_c$  in the LER cavity are shown. They all oscillate coherently with a frequency of approximately 550 Hz. The data is reproduced from Ref. [9].

and  $\psi_H = 10^\circ$  could effectively mitigate the oscillation. Thus, a practical remedy to avoid oscillations was found, although the cause was not fully understood [9]. Following the introduction of the remedy, the oscillation problem did not deteriorate the luminosity performance with the crab crossing. These phase shifts were increased further when the beam currents were increased [10].

In addition to the oscillation problem, the LER tuning system exhibited abnormal behavior; the tuning phase  $\psi_L$  exhibited a large fluctuation of approximately  $\pm 15^\circ$  [8]. The cause of the poor performance of LER tuning system was not clear; one suspected cause was mechanical problems in the tuning system. The abnormal behavior of the LER tuner was also observed in the tuner movement tests performed after assembling the cryostat [19,20]. The tuning method adopted in the KEKB crab cavities [8] involved the adjustment of the insertion depth of the inner conductor of the coaxial coupler, which was originally attached to dampen the lower-order frequency mode [21], into the cavity cell using a stepping motor and piezo. The HER tuning system functioned normally with this tuning method, and  $\psi_H$  was controlled within  $\pm 1^\circ$  of the set value of the loading angle. However, in the LER tuning system, the coupler moved back and forth, passing the set point of the loading angle, resulting in a large periodic fluctuation of  $\psi_L$  with a period of approximately 30 s. The  $V_c$  phase was well-controlled by the PLL with an accuracy of  $\pm 0.1^\circ$  regardless of the periodic fluctuation of  $\psi_L$  [9]. This is considered in the following analysis.

## B. Application of the analysis

The analysis developed in Sec. II was applied to understand the oscillation phenomena observed in KEKB. In the following, the + and - marks for indicating the rings were replaced with *L* (LER) and *H* (HER), respectively.

### 1. Simulation in time domain

First, a time-domain simulation using MATLAB/Simulink [22] was performed based on the formalism developed in the analysis. It aimed to visualize the oscillations of various physical quantities and their relative phases. The consistency between the CE and simulation was confirmed in another study on the stability of the accelerating mode, which has been reported elsewhere [17]. The input data for the simulation were composed based on the system shown in Fig. 2 by identifying each component in  $T_{xk}$  and  $B_{kx}$  of the two rings. The rf control system used in the operation was reflected as accurately as possible in the input data for the simulation.

Figure 8 presents an example of the simulation results. The responses of  $V_c$  amplitude,  $\phi_c$ , and  $\Delta x_{cr}$  to a step change applied to the phase reference at  $t = 0$  are plotted in (a), (b), and (c), respectively. Data for the LER (HER) cavity are plotted in red (blue). The vertical axis represents arbitrary units, and the data in (b) and (c) are plotted with

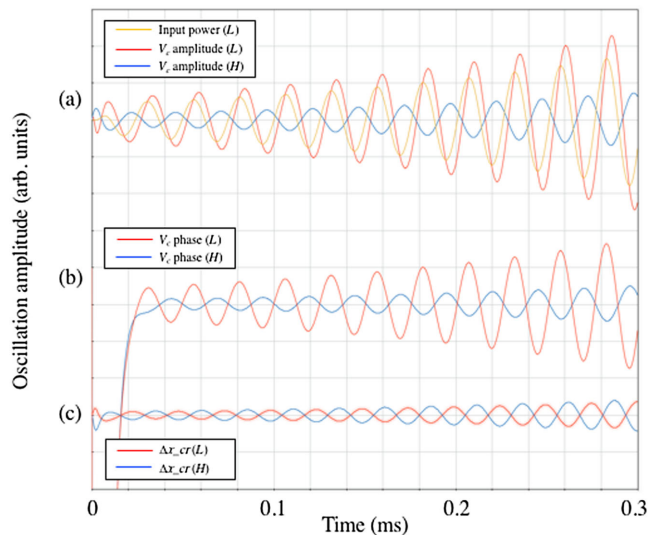


FIG. 8. An example of the time domain simulation performed for KEKB. The responses of  $V_c$  amplitude,  $\phi_c$ , and  $\Delta x_{cr}$  to a step change applied to the phase reference at  $t = 0$  are plotted in (a), (b), and (c), respectively. The vertical axis is in arbitrary unit. The data in the LER (HER) cavity are plotted in red (blue) in each graph. The input power in the LER cavity (green) is also plotted in (a). They all oscillate coherently and grow after the step change.

offsets with respect to (a) for visibility. In (a), the input power  $V_{in}$  in the LER cavity is also plotted (green). They oscillated coherently and grew after the step change. It can be clearly observed that the oscillations were out-of-phase for the two rings. A small phase delay of  $V_c$  with respect to  $V_{in}$  was also observed. These characteristics were consistent with the observed oscillations during the operation, including the data shown in Fig. 7.

### 2. Oscillation amplitude and saturation

Next, the measured data in the machine studies were analyzed. Here, four datasets operated at  $\phi_c$  (in both rings)  $= 90^\circ$  and  $100^\circ$  with  $\psi_H = -10^\circ$  and  $+10^\circ$  were used. Table II shows the quantities measured in the observation [listed in (i)] and the quantities calculated from the data using the analysis [listed in (ii)]. As described above,  $\psi_L$  fluctuated by approximately  $\pm 15^\circ$  in each case, and the values of  $\psi_L$  listed in the table were those obtained when recording the measured data.  $\Delta V_{in}/V_{in(L)}$ ,  $\Delta V_c/V_{c(L)}$ , and  $\Delta \phi_{c(L)}$  are the oscillation amplitudes in the LER cavity in peak-to-peak values, and  $\Delta \phi_{c(H)}/\Delta \phi_{c(L)}$  is the ratio of the  $\phi_c$  oscillation amplitudes in the HER to LER.

From the measured data, the quantities listed in (ii) were calculated following the analysis developed in Sec. II. First,  $\Delta k_{cr}$  was calculated using  $\Delta V_c/V_c$ ,  $\Delta \phi_c$ , and Eq. (19). Subsequently,  $\Delta x_{cr}$  and  $\Delta x^*$  were calculated using  $B_{kx,0}$  values determined by Eq. (18), employing the optics and beam-beam force parameters. Furthermore, by assuming

TABLE II. Four typical datasets of the observed oscillation in the KEKB crab-crossing operation: (i) measured quantities in the observation and (ii) calculated quantities from the measured data by applying the analysis in Sec. II.

Quantity	Unit	Observed data			
		(a)	(b)	(c)	(d)
(i): Measured quantities in the observation					
$\phi_{c(L,H)}$	(deg)	90	90	100	100
$\psi_H$	(deg)	-10	+10	-10	+10
$\psi_L$	(deg)	-2	+6	+4	+18
$\Delta V_{in}/V_{in(L)} (p-p)$		0.05	0.07	0.14	0.31
$\Delta V_c/V_{c(L)} (p-p)$		0.1	0.1	0.14	0.35
$\Delta\phi_{c(L)} (p-p)$	(deg)	2.8	2.8	6.0	8.4
$\Delta\phi_{c(H)}/\Delta\phi_{c(L)}$		-1/2	-1/3	-1/2	-1/3
(ii): Calculated quantities by applying the analysis					
$\Delta x_{cr(L)} (p-p)$	( $\mu\text{m}$ )	-220	-200	-360	-340
$\Delta x_{cr(H)} (p-p)$	( $\mu\text{m}$ )	260	230	430	390
$\Delta x_L^* (p-p)$	( $\mu\text{m}$ )	100	100	160	170
$\Delta x_H^* (p-p)$	( $\mu\text{m}$ )	-50	-34	-82	-57
$\Delta x_{(L-H)}^*$ <sup>a</sup>	( $\mu\text{m}$ )	$\pm 75$	$\pm 67$	$\pm 120$	$\pm 110$
$\Delta V_{br(L)} (p-p)$	(kV)	-26	-23	-42	-39
$\Delta V_{br(H)} (p-p)$	(kV)	13	11	21	20

<sup>a</sup>Defined as  $(\Delta x_L^* - \Delta x_H^*)/2$ .

that the centers of the oscillating orbits were the same as those in the steady state, the relative displacement of the two beams at the IP  $\Delta x_{(L-H)}^*$  was evaluated from the difference between  $\Delta x_L^*$  and  $\Delta x_H^*$ . The variation in the beam-induced voltage on resonance  $\Delta V_{br}$  was also calculated from  $\Delta x_{cr}$ .

The oscillation amplitude remained relatively constant at several degrees of peak-to-peak in  $\phi_c$  for each case and did not increase further. In addition, the calculated values of  $\Delta x_{(L-H)}^*$  for the four measurements from  $\pm 67$  to  $\pm 120$   $\mu\text{m}$  were of the same order as the effective beam size  $\Sigma_x$  calculated using  $\sigma_x^*$  in Table I. These features are consistent with the saturation of the nonlinear beam-beam force. In the linear analysis, once instability occurs, the oscillation grows exponentially with time without limitations, as shown in the simulation results (Fig. 8). However, the linear function of the beam-beam force represented in Eq. (15) is only valid for small values of  $\Delta x_{(L-H)}^*$ . As  $\Delta x_{(L-H)}^*$  increases, the beam-beam force becomes smaller than the linear function. It attains a maximum value at approximately  $\Delta x_{(L-H)}^* = 1.3 \Sigma_x$  for a rigid Gaussian flat beam and decreases at further distances. Consequently, the growth of the oscillation stops at certain value of  $\Delta x_{(L-H)}^*$  where the kick in the crab cavity and the beam-beam force at the IP become balanced, with the growth rate being reduced to zero. An accurate evaluation of the saturation point is difficult because of uncertainties in beam sizes at

the IP with dynamic effects as well as the non-Gaussian distribution of beams. However, the calculated  $\Delta x_{(L-H)}^*$  from the measured oscillation amplitudes were, at least qualitatively, consistent with the nonlinear behavior of the coherent beam-beam force at the IP.

### 3. Loop characteristic analysis

Loop characteristic analysis was performed to study the rf-related parameter dependencies of stability. In Fig. 2, the open-loop overall TF of system  $G_{\text{oval}}$  can be defined by selecting, for example, point  $\Delta x_{cr}^+$  in the LER. By opening the direct transmission from  $\Delta x_{cr}^+$  at the right edge to  $\Delta x_{cr}^+$  at the left edge,  $G_{\text{oval}}$  was defined as the TF between these two points. The sign of  $G_{\text{oval}}$  was reversed for analogy to ordinary feedback loop analysis, such that the CE was expressed as  $1 + G_{\text{oval}} = 0$ .  $G_{\text{oval}}$  comprised the TFs of  $T_{xk}^L$ ,  $T_{xk}^H$ , and a set of  $B_{kx}$ . The forms of  $B_{kx}^{LL}$ ,  $B_{kx}^{LH}$ ,  $B_{kx}^{HL}$ , and  $B_{kx}^{HH}$ , which are the TFs from  $\Delta k_{cr}$  to  $\Delta x_{cr}$ , were obtained from Eqs. (17) and (18). The forms of  $T_{xk}^L$  and  $T_{xk}^H$ , which are the TFs from  $\Delta x_{cr}$  to  $\Delta k_{cr}$ , are represented by Eq. (20). In  $C_p$  and  $C_a$  of  $T_{xk}$ , the time constants and gains of the PLL and ACL used in the operation were set. Subsequently, the Bode diagrams of  $G_{\text{oval}}$  were obtained for the different parameter sets used in the measurements.

There exist certain concerns related to the LER cavity-tuning problem. In addition to the large fluctuation of  $\psi_L$ , the abnormal movement of the coaxial coupler might have caused other issues, such as the distortion of the crabbing field, displacement of the beam orbit with respect to the field axis, and uncertainty of the measured  $\psi_L$ . No further experiments could be conducted to examine these uncertainties because the hardware system had already been disassembled. Therefore, we only discussed the dependencies of stability on  $\phi_c$  and  $\psi_H$  at a fixed value of  $\psi_L = 5^\circ$  because many measurements were conducted in the machine study at this value.

Figure 9 shows the calculated  $\phi_c$  dependence of the loop gain (a) and phase (b) of  $G_{\text{oval}}$ , where  $\phi_c$  was changed from  $86^\circ$  to  $100^\circ$ . Other parameters were set as  $I_{b(L)} = 2$  A,  $I_{b(H)} = 1$  A,  $\psi_L = 5^\circ$ , and  $\psi_H = 0^\circ$ , and the frequency range from 1 to  $10^4$  Hz is plotted. The extremely low gain in the low-frequency region shown in (a) indicates that a possible fluctuation  $\Delta x_{cr(L)}$  is well suppressed by the feedback loops included in  $G_{\text{oval}}$ . This remark is made to avoid confusion with an ordinary feedback loop analysis case, wherein a high open-loop gain in the low-frequency region is usually required to stabilize the closed loop. In the high-frequency region ( $> 10^3$  Hz), the loop gain rapidly decreased with frequency because of the time constant of the cavities  $\tau_f$  in  $B_{kx}$  and that of  $C_p$  and  $C_a$  in  $T_{xk}$ .

We mainly focused on the frequency range of  $10^2$ – $10^3$  Hz, where the loop gain was relatively high. In this region, the loop characteristics are sensitive to

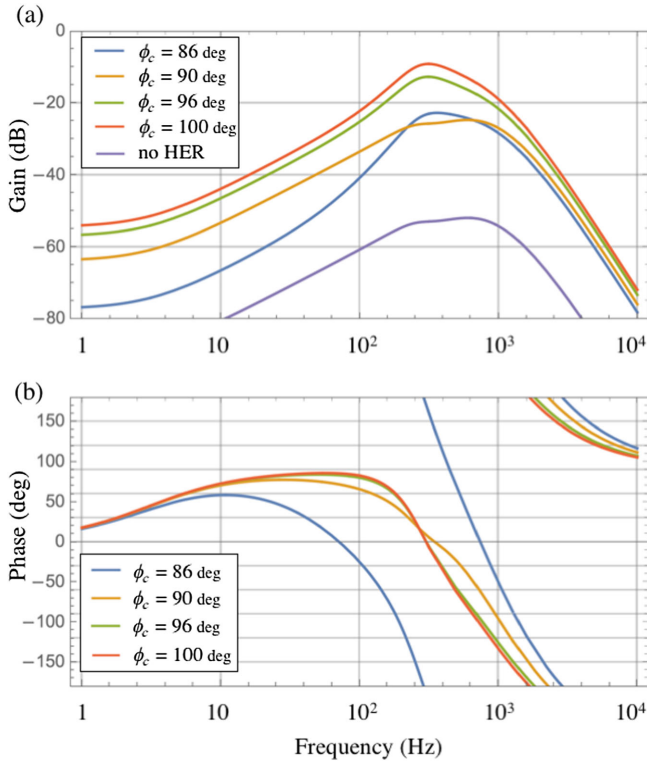


FIG. 9.  $\phi_c$  dependence of the gain (a) and phase (b) for the open loop TF  $G_{\text{oval}}$ . The horizontal axis is frequency from 1 to 10<sup>4</sup> Hz. The vertical axes are the gain in dB (a) and phase in degrees (b), respectively.  $\phi_c = 86^\circ$  (blue),  $\phi_c = 90^\circ$  (orange),  $\phi_c = 96^\circ$  (green), and  $\phi_c = 100^\circ$  (red) are plotted.  $\psi_H = 0^\circ$  and  $\psi_L = 5^\circ$  for all data. The no HER beam case (purple) is also plotted in (a).

rf-related and control parameters. As shown in Fig. 9(b), for  $\phi_c = 86^\circ$  (blue), the loop phase rotated by approximately 360°, passing  $\pm 180^\circ$  through the high-gain region. However, for the  $\phi_c = 90^\circ$ , 96°, and 100° cases, the loop phase remained within approximately  $\pm 100^\circ$  and did not pass  $\pm 180^\circ$  in this frequency region. In Fig. 9(a), the case wherein no beam was stored in the HER is also plotted (purple). As evident, the loop gain with the HER beam increased by 20–40 dB compared to the case without the HER beam. This is because  $B_{kx}^{LL}$  and  $B_{kx}^{HL}$  increased with the HER beam by almost the same factor owing to the beam-beam force at the IP, as well as the contribution from the HER loops. Thus, the effect of the loop phase shift on loop performance was largely enhanced by the colliding beams. Consequently, we conclude that the system is more stable in the  $\phi_c = 90^\circ$ , 96°, and 100° cases than in the  $\phi_c = 86^\circ$  cases.

Similarly, the  $\psi_H$  dependence of the stability was examined. Figure 10 shows the calculated loop gain (a) and phase (b) of  $G_{\text{oval}}$ . In (a),  $\psi_H$  was changed to  $-10^\circ$  (green),  $0^\circ$  (orange), and  $+10^\circ$  (blue), where  $\phi_c = 100^\circ$  and  $\psi_L = 5^\circ$ . The case without an HER beam is shown in red. The other parameters were the same as those in Fig. 9.

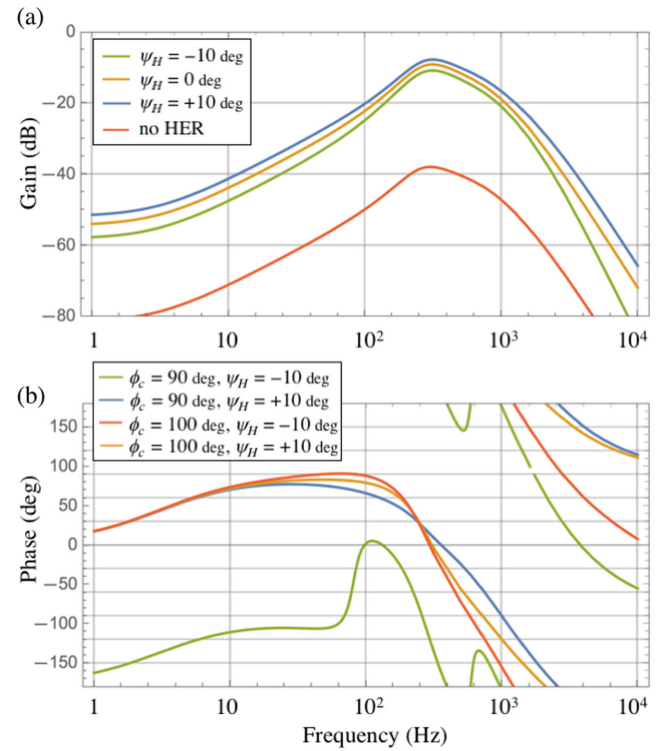


FIG. 10.  $\psi_H$  dependence of the gain (a) and phase (b) for the open loop TF  $G_{\text{oval}}$ . The horizontal axis is frequency from 1 to 10<sup>4</sup> Hz. The vertical axes are the gain in dB (a) and phase in degrees (b), respectively. In (a),  $\psi_H = -10^\circ$  (green),  $\psi_H = 0^\circ$  (orange), and  $\psi_H = 10^\circ$  (blue) are plotted. The no HER beam case (red) is also plotted.  $\phi_c = 100^\circ$  and  $\psi_L = 5^\circ$  for all these data. In (b),  $\psi_H = -10^\circ$  with  $\phi_c = 90^\circ$  (green),  $\psi_H = 10^\circ$  with  $\phi_c = 90^\circ$  (blue),  $\psi_H = -10^\circ$  with  $\phi_c = 100^\circ$  (red), and  $\psi_H = 10^\circ$  with  $\phi_c = 100^\circ$  (orange) are plotted.  $\psi_L = 5^\circ$  for all these data.

The loop gain is relatively high in the frequency range of 10<sup>2</sup>–10<sup>3</sup> Hz, and an enhancement of the loop gain with the HER beam by approximately 30 dB was also observed. In (b), four datasets with changing  $\psi_H$  and  $\phi_c$  are plotted:  $\psi_H = -10^\circ$  with  $\phi_c = 90^\circ$  (green),  $\psi_H = +10^\circ$  with  $\phi_c = 90^\circ$  (blue),  $\psi_H = -10^\circ$  with  $\phi_c = 100^\circ$  (red), and  $\psi_H = +10^\circ$  with  $\phi_c = 100^\circ$  (orange). In the  $\psi_H = -10^\circ$  with  $\phi_c = 90^\circ$  case (green), the loop phase changed significantly, passing  $\pm 180^\circ$  through the high-gain region. In contrast, in the  $\psi_H = +10^\circ$  cases [with  $\phi_c$  of either 90° (blue) or 100° (orange)], the phase change was relatively modest. Consequently, we conclude that the system is more stable with  $\psi_H = +10^\circ$  than with  $\psi_H = -10^\circ$ .

In addition, by comparing the two cases marked by green and red in (b), the system is more stable with  $\phi_c = 100^\circ$  than with  $\phi_c = 90^\circ$  at the same value of  $\psi_H = -10^\circ$ . This does not conflict with the  $\phi_c$  dependence of stability discussed previously in Fig. 9.

To understand the loop phase change depending on  $\phi_c$  and  $\psi$ , it is helpful to recall the forms of  $C_p$  and  $C_a$  for simple cases wherein only the PLL or ACL is implemented,

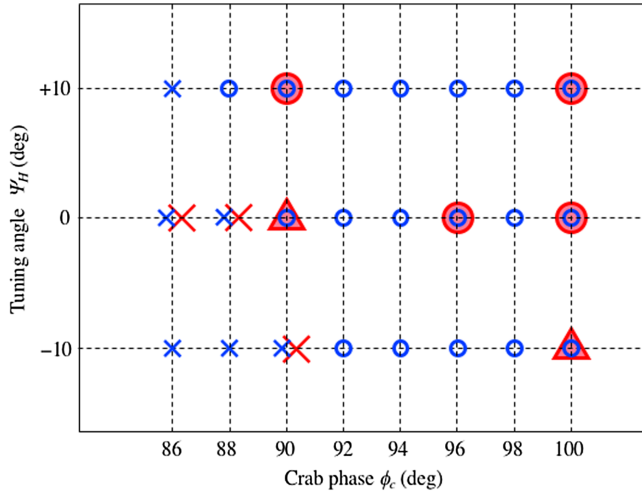


FIG. 11. Comparison between the calculation and measurement results of the  $\phi_c$  and  $\psi_H$  dependencies of stability. The horizontal and vertical axes are  $\phi_c$  and  $\psi_H$ , respectively. The calculated results are plotted according to their phase patterns: unstable (blue crosses) and stable (blue open circles). The measurement results are plotted according to whether the instability was observed (red crosses), not observed (red circles), or marginal (red triangles).

as presented in Sec. II C. Because  $\phi_c$  is close to  $90^\circ$ , the sign of the coefficient of  $C_p$  in Eq. (23) is sensitive to  $\phi_c$ . Similarly, the sign of the coefficient of  $C_a$  in Eq. (24) is sensitive to  $(\phi_c - \psi)$ .

Figure 11 presents a comparison of the calculation and measurement results of  $\phi_c$  (horizontal axis) and  $\psi_H$  (vertical axis) dependencies of stability. The calculated results are plotted by classifying the data into two groups according to their phase patterns: unstable (blue crosses) and stable (blue open circles). The measurement data are plotted and classified into three groups: instability was observed (red crosses), not observed (red circles), or marginal (red triangles). In both the calculations and measurements, the data were obtained at a fixed value of  $\psi_L = 5^\circ$ . As evident, the  $\phi_c$  and  $\psi_H$  dependencies obtained in the loop characteristic analysis and the measured values were consistent.

## V. DISCUSSIONS

We investigated the stability of the crab rf systems with colliding beams. We developed an analysis method by formulating the TFs of a crab system, comprising the beam-beam force at the IP, beam loading on crab cavities, and rf control loops. The analysis was first applied to simple cases without control loops, and the intrinsic stability criteria were identified as functions of  $Y'\kappa B_{kx,0}$  (or  $I_b$ ) and the tuning angle  $\psi$ .

Next, the analysis, including the control loops, was applied to study the oscillation phenomena observed during the crab-crossing operation in KEKB. The calculations and

measurements were consistent with the following points: First, the time-domain simulation reproduced the characteristics of the observed oscillations. Coherent oscillations of  $V_c$  amplitude,  $\phi_c$ , and  $\Delta x_{cr}$  were observed, and the relative phase between these quantities in the two rings were consistent with that in the measurements. Second,  $\Delta x_{(L-H)}^*$  estimated from the measured oscillation amplitude by applying the analysis was consistent with the saturation effect of the beam-beam force at the IP. Third, the  $\phi_c$  and  $\psi_H$  dependencies of the stable and unstable conditions obtained by the loop characteristic analysis were consistent with those in the measurements.

Although these consistencies indicated the validity of the analysis, there were certain discrepancies between the calculations and measurements. First, during operation, instability was usually observed at lower beam currents, that is, a factor of approximately two, compared to the calculated threshold currents. Second, the measured oscillation frequency was roughly fixed at 550 Hz regardless of the different values of the rf parameters, such as  $\phi_c$  and  $\psi$ , and the control loop parameters.

To understand the cause of these discrepancies, the possible effects of the two known coherent phenomena and bunch-gap transient were examined. One is ordinary coupled-bunch instability (CBI) arising from crab cavities. Owing to the high transverse impedance of the crab cavities, a transverse CBI can be excited by the off-peak of the impedance spectrum around the rf frequency, reaching the driving frequency of the instability. The growth rate of the coupled-bunch mode  $m$ ,  $\tau_{(m)}^{-1}$ , is expressed as

$$\tau_{(m)}^{-1} = \frac{eI_b f_{\text{rev}} \beta_{cr}}{2E} (\text{Re}Z_{(m)}^+ - \text{Re}Z_{(m)}^-), \quad (35)$$

where  $f_{\text{rev}} = 1/\tau_{\text{rev}}$  is the revolution frequency, and  $\text{Re}Z_{(m)}^+$  ( $\text{Re}Z_{(m)}^-$ ) is the real part of the impedance of the crab cavity at the driving (damping) frequency of mode  $m$ .  $\text{Re}Z_{(m)}^\pm$  is represented as

$$\text{Re}Z_{(m)}^\pm = \frac{\frac{1}{2} \left(\frac{R}{Q}\right) k_{rf} Q_L}{1 + [\tan \psi \pm \frac{2\pi}{\sigma} (m + N_\beta + \nu_\beta) f_{\text{rev}}]^2}, \quad (36)$$

where  $N_\beta$  and  $\nu_\beta$  are the integer and fractional parts of the transverse tune, respectively.

Two modes,  $m' \equiv m + N_\beta = 0$  ( $0'$  mode) and  $-1$  ( $-1'$  mode), whose driving frequencies are close to the rf frequency, can exhibit a high growth rate. The growth rate was calculated using the parameters of KEKB-LER listed in Table I except that the beam current was set to 2 A, which is considerably higher than the operating current. The results are presented in Fig. 12, where  $\tau^{-1}$  of the two dominant modes  $0'$  and  $-1'$  are plotted as blue and red real lines, respectively, as a function of  $\psi_L$ . Even with the fluctuation of  $\psi_L$  by  $\pm 15^\circ$  caused by the tuning problem, the operation was always performed in the range of

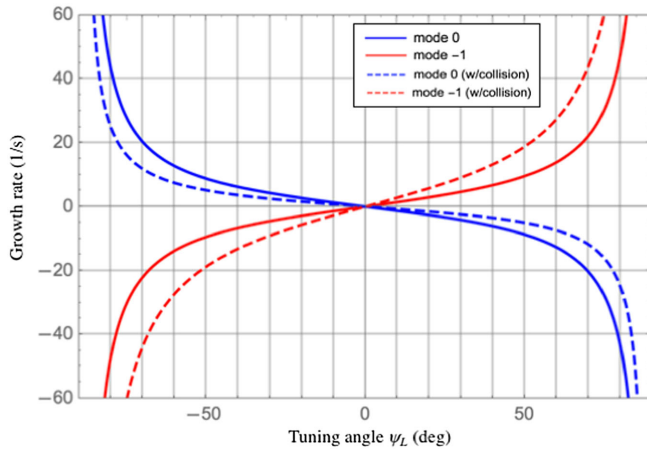


FIG. 12. The growth rate  $\tau^{-1}$  of ordinary coupled-bunch instability (CBI) caused by a crab cavity in KEKB-LER as a function of  $\psi_L$ . Two modes,  $m' \equiv m + N_\beta = 0$  ( $0'$  mode) and  $-1$  ( $-1'$  mode), whose driving frequencies are close to the rf frequency, are plotted as blue and red, respectively. The dashed lines consider the tune shift  $\Delta\nu_\beta \sim 0.1$  to simply model the effect of coherent beam-beam force at the IP on the CBI.

$|\psi_L| < 30^\circ$ . Larger values of  $|\psi_L|$  would increase the input power needed to maintain  $V_c$ . In this range of  $\psi_L$ ,  $\tau^{-1}$  was less than the radiation damping rate ( $\sim 25 \text{ s}^{-1}$ ).

The CBI discussed for a single ring should be modified for colliding beams because of the beam-beam force at the IP. This effect was approximated as a shift of  $\nu_\beta$  on the order of the coherent tune shift  $\Xi_x$ . In Fig. 12,  $\tau^{-1}$  modified with  $\Delta\nu_\beta \sim 0.1$  is plotted as dashed lines. Although  $\tau^{-1}$  of the  $-1'$  mode (red dashed line) increased for  $\psi_L > 0$ ,  $\tau^{-1} < 10 \text{ s}^{-1}$  for  $|\psi_L| < 30^\circ$ . Even if  $\tau^{-1}$  were to increase by certain unknown effects, such as machine errors or other instability sources, it would be probably sufficiently lower than the damping rate of the transverse bunch-by-bunch feedback system implemented in KEKB, which is of the order of  $10^3 \text{ s}^{-1}$ .

Another possibility is the effect of the coherent synchrotron frequency shift caused by the beam loading on the accelerating cavities. As described in Sec. II A, the beam phase is determined by the accelerating rf system. When coherent synchrotron oscillation occurs, the beam phase changes accordingly and the crabbing field  $V_c$  is affected by the TFs from  $p_b$  to  $V_c$ . However, this effect was not considered in this analysis. The coherent synchrotron frequency  $f_s$  was calculated with the parameters listed in Table I, by using a simulation tool developed for the accelerating rf system [17]. The results showed that  $f_s$  in the LER (HER) shifted from 2.44 (2.08) kHz at zero current to 2.05 (1.47) kHz at the operating currents. The frequencies were significantly higher than the observed oscillation frequency of approximately 550 Hz. Consequently, the coherent synchrotron frequency shift did not appear to be related to the observed instability.

Next, the effect of the bunch-gap transient was examined. In KEKB, a gap with empty buckets occupying approximately 5% of the ring was introduced in the bunch train to allow for the rise time of the beam abort kicker. Owing to the gap transient effect, the bunch-pass timing (i.e., the synchronous phase  $\phi_s$ ) changes bunch-by-bunch along the train. The collision point shifts longitudinally according to the relative displacements of the colliding bunches in the two beams. This results in the relative horizontal displacement of the colliding bunches  $\Delta x_{(L-H)}^*$  in a finite-angle crossing scheme. The effect of the bunch-gap transient was studied for noncrab finite-angle crossings in KEKB, which has been reported elsewhere [23,24].  $\Delta\phi_s$  and  $\Delta x_{(L-H)}^*$  in the KEKB operation were estimated to be several degrees and of the order of  $10 \text{ }\mu\text{m}$ , respectively.

In the crab-crossing case, two points should be added to the argument above. First, the longitudinal collision point shift by itself does not result in a relative horizontal displacement because of head-on collisions owing to the crab crossing. However, different bunch-pass timings in the crab cavity cause different horizontal kicks  $\Delta k_{cr} \sim \kappa \Delta\phi_s$ ; therefore,  $\Delta x_{cr}$  and  $\Delta x^*$  change bunch-by-bunch along the train. Using Eq. (16) with the KEKB parameters,  $\Delta x_{cr}$  was estimated to be of the order of  $100 \text{ }\mu\text{m}$ , and  $\Delta x^*$  was several tens  $\mu\text{m}$ . In most parts of the train,  $\Delta x^*$  of the colliding bunches were in the same direction between the two beams, which reduced  $\Delta x_{(L-H)}^*$  to a few tens  $\mu\text{m}$  by canceling it out. Second, the beam loading on the crab cavity of a bunch train should be calculated by superposing that of a single bunch with factors  $\cos \Delta\phi_s$  and  $\Delta x_{cr}$  for each bunch. In the KEKB case, this superposition can be approximated by using the average values of  $\Delta x_{cr}$  and  $\phi_s$  along the train. In addition, the time constant of the gap transient effect is typically  $\tau_{rev}$  ( $10 \text{ }\mu\text{s}$ ), which is significantly shorter than the oscillation period ( $\sim 200 \tau_{rev}$ ). Based on these considerations, we conclude that the bunch-gap transient effect was not related to the instability observed in KEKB.

Regarding the instability arising at beam currents lower than the calculated predictions, it may be argued that, as shown in Figs. 9 and 10, a gain margin exists even at the frequency where the loop phase crosses  $\pm 180^\circ$ . However, from experience in machine operations, the gain margin can be lost owing to a variety of factors that impede the ideal situation, such as nonlinearities in the rf system, unknown fluctuations in the hardware system, and the degradation of beam dynamics caused by machine errors. For example, in the early stage of the KEKB operation without crab cavities, the  $-1$ -mode longitudinal instability associated with the accelerating mode occurred at approximately half of the beam current predicted via calculations [25].

According to the loop performance analysis, the stability can be degraded in the frequency range of approximately 400–700 Hz because of the relatively high loop gain caused by the beam loading on the crab cavities and the beam-beam force at the IP. The frequency where the loop phase

reaches  $\pm 180^\circ$  could change in this frequency range, depending on the values of the different parameters. Thus, the observed frequency, which was roughly fixed at 550 Hz, cannot be explained by the loop performance alone. One emerging possibility is that an unknown oscillation source at approximately 550 Hz may have existed in the rf system, power supply, or crab cavity, which did not affect the stability in the case of a noncrab collision operation. A relatively high noise floor was often observed around this frequency during operation, even at a low beam current. Although the noise source was not identified, it could have been enhanced by the loop performance with the interaction between the beam loading on crab cavities and the beam-beam force at the IP, as studied in our analysis.

## VI. SUMMARY

We investigated the coherent instability in the crab-crossing collision, which is caused by an interaction between the beam loading on the crab cavities and the beam-beam force at the IP. We developed an analysis method to study the stability by formulating TFs for a crab rf system with colliding beams, comprising the beam loading on crab cavities, beam orbit response to the crab kick with the beam-beam force at the IP, and rf control loops for the amplitude and phase of  $V_c$ .

The analysis was first applied to simple cases without control loops to derive the intrinsic stability. This corresponds to the Robinson stability for accelerating cavities. Two cases were examined: The first was the case wherein every machine parameter was identical for the two rings. The second was with the KEKB parameters as an example of a more general case wherein the machine parameters were different between the two rings. Stability criteria were identified for both cases.

Furthermore, analysis with the control loops was applied to study the instability observed during the crab-crossing operation in KEKB. The calculation and measurement

results were consistent with the following points. First, a time-domain simulation based on the analysis reproduced the coherent oscillation in the two rings observed during operation. Second, the relative beam orbit displacement at the IP estimated from the measured data by applying the analysis was consistent with the saturation effect of the beam-beam force. Third, the  $\phi_c$  and  $\psi_H$  dependencies of the stable and unstable conditions were consistent between the loop characteristic analysis and the measurements.

However, there were certain discrepancies between the calculations and measurements. In the operation, instability usually occurred at beam currents lower than those predicted by the calculation, and the oscillation frequency was approximately fixed. Nevertheless, in the mechanism studied here, the interaction between the beam loading on the crab cavities and the beam-beam force at the IP could increase the effect of certain noise sources, if any, by more than 30 dB. In addition, nonlinearities in the rf system, fluctuations in the hardware system, and beam dynamics issues that are caused by machine errors could affect the loop performance. Considering these factors, we confirmed the validity of the analysis developed in this study and its essential function in the instability observed in the crab-crossing operation in KEKB.

## ACKNOWLEDGMENTS

The author would like to thank KEKB accelerator staff, particularly the commissioning group, the crab cavity and refrigerator group, and the rf group, for their cooperation in the design, construction, and operation of the crab crossing in KEKB.

## APPENDIX A: TF FROM GENERATOR TO CAVITY

The TFs from the generator to the crabbing voltage were obtained from the transformation of  ${}^t(a_g, p_g)$  into  ${}^t(a_v, p_v)$  in Eq. (2) as

$$G_{pp}^G = G_{aa}^G = \frac{\sigma(1 + Y^* \sin \phi_c) \cdot s + \sigma^2 [\sec^2 \psi + Y^* (\sin \phi_c - \tan \psi \cos \phi_c)]}{s^2 + 2\sigma s + \sigma^2 \sec^2 \psi}, \quad (\text{A1})$$

$$G_{ap}^G = -G_{pa}^G = \frac{\sigma(-\tan \psi + Y^* \cos \phi_c) \cdot s + \sigma^2 Y^* (\cos \phi_c + \tan \psi \sin \phi_c)}{s^2 + 2\sigma s + \sigma^2 \sec^2 \psi}. \quad (\text{A2})$$

Note that they are similar to those for accelerating cavities [13,17], with differences in the beam-loading coefficients and relative phase between the rf and beam:  $Y^*$  in Eqs. (A1) and (A2) are given by Eq. (9), whereas  $Y$ , which appears in the form of

accelerating cavities, is defined as  $Y = (R/Q)Q_L I_b / V_c$ . In addition,  $\phi_c$  used in Eqs. (A1) and (A2) is the crabbing phase, whereas for the accelerating cavities,  $\phi_c$  is replaced by  $\phi_s + \pi/2$ , where  $\phi_s$  is the synchronous phase.

### APPENDIX B: $B_{kx,0}$ FOR TWO RINGS WITH THE IDENTICAL PARAMETERS

Using Eqs. (13) and (15) in Sec. III, the  $4 \times 4$  matrix  $I - T$  is expressed as

$$I - T = \begin{pmatrix} \mathbf{I} & \mathbf{0} \\ \mathbf{0} & \mathbf{I} \end{pmatrix} - \begin{pmatrix} \mathbf{M}_{11} & \mathbf{0} \\ \mathbf{0} & \mathbf{M}_{11} \end{pmatrix} - f_b \begin{pmatrix} -\mathbf{W} & \mathbf{W} \\ \mathbf{W} & -\mathbf{W} \end{pmatrix}, \quad (\text{B1})$$

where  $\mathbf{M}_{11}$  is the one-turn matrix at the crab cavity,  $f_b = 4\pi\Xi_x/\beta_x^*$ , and

$$\mathbf{W} = \begin{pmatrix} \mathbf{M}_{21(1,2)}\mathbf{M}_{12(1,1)} & \mathbf{M}_{21(1,2)}\mathbf{M}_{12(1,2)} \\ \mathbf{M}_{21(2,2)}\mathbf{M}_{12(1,1)} & \mathbf{M}_{21(2,2)}\mathbf{M}_{12(1,2)} \end{pmatrix}. \quad (\text{B2})$$

Let the matrix  $(I - T)^{-1}$  be represented by  $2 \times 2$  matrices as

$$(I - T)^{-1} = \begin{pmatrix} \mathbf{A} & \mathbf{B} \\ \mathbf{C} & \mathbf{D} \end{pmatrix},$$

then from Eq. (B1) we obtain

$$\mathbf{A} = (\mathbf{I} - \mathbf{M}_{11} + 2f_b\mathbf{W})^{-1} \times [f_b\mathbf{W}(\mathbf{I} - \mathbf{M}_{11})^{-1} + \mathbf{I}],$$

$$\mathbf{B} = (\mathbf{I} - \mathbf{M}_{11} + 2f_b\mathbf{W})^{-1} \times [f_b\mathbf{W}(\mathbf{I} - \mathbf{M}_{11})^{-1}].$$

From the optics parameters at the crab cavity and the IP, the components of  $(\mathbf{I} - \mathbf{M}_{11})^{-1}$  and  $\mathbf{W}$  in Eq. (B2) are expressed as

$$(\mathbf{I} - \mathbf{M}_{11})^{-1} = \frac{1}{4\sin^2(\frac{\phi_0}{2})} \times \begin{pmatrix} 1 - \cos \phi_0 + \alpha_{cr} \sin \phi_0 & \beta_{cr} \sin \phi_0 \\ -\gamma_{cr} \sin \phi_0 & 1 - \cos \phi_0 - \alpha_{cr} \sin \phi_0 \end{pmatrix},$$

$$\mathbf{W}_{(1,1)} = \beta^* \cos \varepsilon_{21} (-\sin \varepsilon_{12} + \alpha_{cr} \cos \varepsilon_{12}),$$

$$\mathbf{W}_{(1,2)} = \beta^* \beta_{cr} \cos \varepsilon_{21} \cos \varepsilon_{12},$$

$$\mathbf{W}_{(2,1)} = \frac{\beta^*}{\beta_{cr}} (\sin \varepsilon_{21} + \alpha_{cr} \cos \varepsilon_{21}) (\sin \varepsilon_{12} - \alpha_{cr} \cos \varepsilon_{12}),$$

$$\mathbf{W}_{(2,2)} = \beta^* \cos \varepsilon_{12} (-\sin \varepsilon_{21} - \alpha_{cr} \cos \varepsilon_{21}).$$

The components of  $\mathbf{H} \equiv (\mathbf{I} - \mathbf{M}_{11} + 2f_b\mathbf{W})^{-1}$  are obtained as

$$h\mathbf{H}_{(1,1)} = 1 - \cos \phi_0 + \alpha_{cr} \sin \phi_0 - 2f_b\beta^* \cos \varepsilon_{12} (\sin \varepsilon_{21} + \alpha_{cr} \cos \varepsilon_{21}),$$

$$h\mathbf{H}_{(1,2)} = \beta_{cr} \sin \phi_0 - 2f_b\beta^* \beta_{cr} \cos \varepsilon_{21} \cos \varepsilon_{12},$$

$$h\mathbf{H}_{(2,1)} = -\gamma_{cr} \sin \phi_0 - 2f_b \frac{\beta^*}{\beta_{cr}} (\sin \varepsilon_{21} + \alpha_{cr} \cos \varepsilon_{21}) \times (\sin \varepsilon_{12} - \alpha_{cr} \cos \varepsilon_{12}),$$

$$h\mathbf{H}_{(2,2)} = 1 - \cos \phi_0 - \alpha_{cr} \sin \phi_0 - 2f_b\beta^* \cos \varepsilon_{21} (\sin \varepsilon_{12} - \alpha_{cr} \cos \varepsilon_{12}),$$

with  $h \equiv \det \mathbf{H}^{-1}$  being

$$h = 2(1 - \cos \phi_0 + \beta^* f_b \sin \phi_0).$$

Finally,  $\mathbf{A}$  and  $\mathbf{B}$  are calculated, yielding Eqs. (33) and (34), as follows:

$$B_{kx,0} = \mathbf{A}_{(1,2)}, \quad (\text{B3})$$

$$\eta = \mathbf{B}_{(1,2)}/\mathbf{A}_{(1,2)}. \quad (\text{B4})$$

- 
- [1] R. B. Palmer, Energy scaling, crab crossing and the pair problem, Stanford Linear Accelerator Center Report No. SLAC-PUB-4707, 1988.
  - [2] K. Oide and K. Yokoya, Beam-beam collision scheme for storage-ring colliders, *Phys. Rev. A* **40**, 315 (1989).
  - [3] K. Ohmi, M. Tawada, Y. Cai, S. Kamada, K. Oide, and J. Qiang, Beam-beam limit in  $e^+e^-$  circular colliders, *Phys. Rev. Lett.* **92**, 214801 (2004).
  - [4] K. Ohmi, K. Oide, and E. A. Perevedentsev, The beam-beam limit and the degree of freedom, in *Proceedings of the 10th European Particle Accelerator Conference, Edinburgh, Scotland, 2006* (JACoW, Geneva, 2006), p. 616.
  - [5] KEKB B-Factory Design Report, KEK Report No. 95-7, 1995.
  - [6] Y. Funakoshi, T. Abe, K. Akai, M. Akemoto, A. Akiyama, M. Arinaga, K. Ebihara, K. Egawa, A. Enomoto, J. Flanagan *et al.*, Performance of KEKB with crab cavities, in *Proceedings of the 11th European Particle Accelerator Conference, Genoa, Italy, 2008*, p. 1893 (JACoW, Geneva, 2008).
  - [7] T. Abe, K. Akai, Y. Cai, K. Ebihara, K. Egawa, A. Enomoto, J. Flanagan, H. Fukuma, Y. Funakoshi, K. Furukawa *et al.*, Commissioning of KEKB, *Prog. Theor. Exp. Phys.* **2013**, 03A010 (2013).
  - [8] K. Hosoyama, K. Hara, A. Honma, A. Kabe, Y. Kojima, Y. Morita, H. Nakai, K. Nakanishi, K. Akai, K. Ebihara, T. Furuya, S. Mitsunobu, M. Ono, Y. Yamamoto, K. Okubo, K. Sennyu, H. Hara, and T. Yanagisawa, Construction and commissioning of KEKB superconducting crab cavities, in *Proceedings of the 13th International Conference on RF Superconductivity, Beijing, China, 2007* (JACoW, Geneva, 2007), p. 63.

- [9] K. Akai, K. Ebihara, T. Furuya, K. Hara, T. Honma, K. Hosoyama, A. Kabe, Y. Kojima, S. Mitsunobu, Y. Morita, H. Nakai, K. Nakanishi, M. Ono, and Y. Yamamoto, Commissioning and beam operation of KEKB crab rf system, in *Proceedings of the 13th International Conference on RF Superconductivity, Beijing, China, 2007* (JACoW, Geneva, 2007), p. 632.
- [10] Y. Yamamoto, K. Akai, K. Ebihara, T. Furuya, K. Hara, T. Honma, K. Hosoyama, A. Kabe, Y. Kojima, S. Mitsunobu, Y. Morita, H. Nakai, K. Nakanishi, M. Ono, and T. Kanekiyo, Beam commissioning status of superconducting crab cavities in KEKB, in *Proceedings of the 1st International Particle Accelerator Conference, Kyoto, Japan, 2010* (JACoW, Geneva, 2020), p. 2444.
- [11] K. W. Robinson, Stability of beam in radiofrequency system, Cambridge Electron Accelerator Report No. CEAL-1010, 1964.
- [12] T. Abe, K. Akai, M. Akemoto, A. Akiyama, M. Arinaga, K. Ebihara, K. Egawa, A. Enomoto, J. Flanagan, S. Fukuda *et al.*, Compensation of the crossing angle with crab cavities at KEKB, in *Proceedings of the 22nd Particle Accelerator Conference, Albuquerque, New Mexico, USA, 2007* (JACoW, Geneva, 2007), p. 27.
- [13] F. Pedersen, Beam loading effects in the CERN PS booster, *IEEE Trans. Nucl. Sci.*, **22**, 1906 (1975).
- [14] K. Hirata, The beam-beam interaction: Coherent effects, *AIP Conf. Proc.*, **214**, 175 (1990).
- [15] K. Ohmi, R. Tomas, Y. Funakoshi, R. Calaga, T. Ieiri, Y. Morita, K. Nakanishi, K. Oide, Y. Ohnishi, Y. Sun, M. Tobiyama, and F. Zimmermann, Response of colliding beam-beam system to harmonic excitation due to crab-cavity rf phase modulation, *Phys. Rev. ST Accel. Beams* **14**, 111003 (2011).
- [16] M. Arinaga, J. W. Flanagan, H. Fukuma, T. Furuya, S. Hiramatsu, H. Ikeda, H. Ishii, E. Kikutani, T. Mitsuhashi, K. Mori, M. Tejima, and M. Tobiyama, Progress in KEKB beam instrumentation systems, *Prog. Theor. Exp. Phys.* **2013**, 03A007 (2013).
- [17] K. Akai, Stability analysis of rf accelerating mode with feedback loops under heavy beam loading in SuperKEKB, *Phys. Rev. Accel. Beams* **25**, 102002 (2022).
- [18] K. Akai and Y. Funakoshi, Beam-loading issues and requirements for the KEKB crab rf system, in *Proceedings of the 5th European Particle Accelerator Conference, Barcelona, Spain, 1996* (JACoW, Geneva, 1996), p. 2118.
- [19] A. Kabe (private communication).
- [20] Y. Yamamoto, K. Akai, K. Ebihara, T. Furuya, K. Hara, T. Honma, K. Hosoyama, A. Kabe, Y. Kojima, S. Mitsunobu, Y. Morita, H. Nakai, K. Nakanishi, M. Ono, H. Hara, K. Sennyu, T. Yanagisawa, T. Kanekiyo, and T. Nakazato, Horizontal tests for crab cavities in KEKB, in *Proceedings of the 13th International Conference on RF Superconductivity, Beijing, China, 2007* (JACoW, Geneva, 2007), p. 520.
- [21] K. Akai, J. Kirchgessner, D. Moffat, H. Padamsee, J. Sears, T. Stowe, and M. Tigner, Crab cavity for the B-factories, Proc. B Factories, SLAC, U. S. A., Report No. SLAC-400, 1992, p. 181.
- [22] MATLAB/Simulink® by The MathWorks, Inc.
- [23] K. Akai, N. Akasaka, K. Ebihara, E. Ezura, M. Suetake, and S. Yoshimoto, The low-level rf system for KEKB, in *Proceedings of the 6th European Particle Accelerator Conference, Stockholm, Sweden, 1998* (JACoW, Geneva, 1998), p. 1749.
- [24] T. Kobayashi and K. Akai, Advanced simulation study on bunch gap transient effect, *Phys. Rev. Accel. Beams* **19**, 062001 (2016).
- [25] S. Yoshimoto, K. Akai, and E. Ezura, The  $-1$  mode damping system for KEKB, in *Proceedings of the 14th Symposium on Accelerator Science and Technology, Tsukuba, Japan, 2003* (2003), p. 323.